POLITECNICO DI TORINO
Repository ISTITUZIONALE

Diffusive memristors in the edge of chaos

Original
Diffusive memristors in the edge of chaos / Ju Kim, S., Wang, T., Zhao, R., Rossetti, D., Xu, Y., Zhao, J., Ascoli, A., Corinto, F., Stanley Williams, R., Joshua Yang, J.. - In: NATURE COMMUNICATIONS. - ISSN 2041-1723. - 17:1(2026). [10.1038/s41467-026-74640-6]

Availability:
This version is available at: 11583/3014854 since: 2026-08-25T18:49:09Z

Publisher:
Nature

Published
DOI:10.1038/s41467-026-74640-6

Terms of use:

This article is made available under terms and conditions as specified in the corresponding bibliographic description in the repository

Publisher copyright

(Article begins on next page)

20 November 2026

nature communications

Article

https://doi.org/10.1038/s41467-026-74640-6

Diffusive memristors in the edge of chaos

Received: 27 September 2025

Accepted: 9 June 2026

Published online: 24 June 2026

Check for updates

Seung Ju Kim[1], Tong Wang[1], Ruoyu Zhao[1], Davide Rossetti[1,2], Yichun Xu[1], Jian Zhao[1], Alon Ascoli[2], Fernando Corinto[2], R. Stanley Williams[1] ✉ & J. Joshua Yang[1] ✉

Biological nervous systems are theorized to operate in the edge of chaos (EOC), a stable and locally active regime enabling energy-efficient information processing. Electronic implementations of such behavior have mainly relied on electrothermal phase transitions, which are power-intensive and unlike biological dynamics. Diffusive memristors, by contrast, harness ionic drift and diffusion resembling biological dynamics, yet their potential for EOC operation has remained unexplored. Here, we experimentally demonstrate ionically moderated EOC behavior in diffusive memristors. At the hundred-nanoampere level, the device exhibits sharp negative differential resistance (NDR) enhanced by a Ridley entropy production minimization transition, noise amplification and spontaneous oscillatory dynamics consistent with operation near the EOC. These emergent behaviors arise from coupled ionic transport, filament evolution and circuit dynamics, as confirmed by compact modeling. This system achieves power efficiency over three orders of magnitude greater than electrothermal EOC devices, introducing low-power neuromorphic elements that emulate brain-like dynamics through nanoionics.

Biological nervous systems acquire and process information far more efficiently than any existing digital electronic hardware. A prevailing hypothesis is that this exceptional efficiency stems from the operation of biological information-processing systems in the 'edge of chaos' (EOC), a dynamical regime associated with enhanced computational capability and adaptability. In the mathematical framework introduced by Chua[1], the EOC is rigorously interpreted through the theory of local activity, where it corresponds to a stable yet locally active operating condition rather than as the onset of deterministic chaos. Under this definition, EOC is a globally stable operating region characterized by small-signal instability and fluctuation amplification, in contrast to concepts based on Lyapunov exponent criteria. A detailed discussion contrasting these two interpretations of EOC is provided in Supplementary Note 1, with Lyapunov exponent results presented in Supplementary Table 1 and Supplementary Figs. 1–4.

A canonical manifestation of such nonlinear dynamics in biological systems is neuronal spiking[2]. As captured by the Hodgkin–Huxley framework[3], neurons exhibit excitability and sensitivity near threshold, where small perturbations can trigger large, all-or-none responses. This regime enables adaptive and robust information encoding while preventing rigid dynamical locking, illustrating how biological systems exploit nonlinear dynamics to balance stability and responsiveness. Foundational analyses of balanced excitatory-inhibitory networks[4] and computational studies of recurrent neural circuits propose that such systems operate near critical dynamical regimes associated with enhanced computational capability[5,6]. Recent reviews further report that large-scale cortical activity exhibits signatures consistent with near-critical behavior that may facilitate efficient information processing[7,8].

Substantial efforts have sought to emulate biologically inspired nonlinear dynamics in electronic systems[9–16]. Especially, electrothermal materials such as VO_2 and NbO_2 have been widely explored[17–19]. These devices utilize Joule self-heating to activate local thermal dynamics, which in turn can induce negative differential resistance (NDR) via feedback with a strongly nonlinear temperature-dependent conductance[20,21]. For example, VO_2 undergoes a Mott insulator-to-metal transition, for which the temperature acts as a dynamical state variable[22]. When coupled with the dynamics of intrinsic or extrinsic circuit capacitances, the resulting second-order differential equation can produce self-sustained oscillations of both

[1]Ming Hsieh Department of Electrical and Computer Engineering, University of Southern California, Los Angeles, CA, USA. [2]Department of Electronics and Telecommunications Engineering, Politecnico di Torino, Turin, Italy. ✉e-mail: rw_841@usc.edu; jjoshuay@usc.edu

voltage and temperature when the memristor is current-biased in the NDR regime of its *V* vs. *I* curve, which has been shown to be a signature of Chua EOC[23]. These devices have demonstrated promise for applications such as action potentials, sources of chaotic dynamics, axon-like active signal transmission, and many other biologically relevant behaviors[24].

Despite these advances, electrothermal mechanisms differ fundamentally from the ionic transport processes central to biological functionality. They rely on thermal activation, typically requiring elevated temperatures sustained by significant DC power dissipation, potentially limiting energy efficiency and scalability. These limitations motivate the exploration of alternative physical mechanisms capable of reproducing nonlinear dynamical behaviors with minimal thermal activation.

Diffusive memristors provide a fundamentally distinct physical platform characterized by the formation of partial metallic filaments from ionic drift and their spontaneous dissolution via atomic diffusion, resulting in volatile resistance states[25–27]. In Ag-based devices, which are representative diffusive memristors, silver ions migrate under an electric field to form conductive channels[28,29], which dissolve back into the matrix when the field is removed. This enables rich dynamic behavior, and such devices have been used in leaky integrate-and-fire (LIF) circuits[30], memory element selectors[31], and threshold detection applications[32,33] when connected with other devices. However, whether diffusive memristors can operate in the EOC on their own has not been previously demonstrated, and the mechanisms that could enable such behavior remain unclear. This uncertainty was further compounded by the interplay between nonlinear dynamics and non-equilibrium thermodynamics, making it difficult to fully understand, with limited efforts to integrate these perspectives[23,34–36].

In this study, we report that an ionic diffusive memristor can operate in the EOC regime, as evidenced by the experimental observation of excitability and fluctuation amplification enabled by a sharp current-controlled Ridley transition[37]. The transition produces a pronounced NDR accompanied by reduced steady-state power dissipation with increasing current, revealing a critical link between nonlinear dynamics and non-equilibrium thermodynamics. These observations further suggest that entropy production minimization, as discussed by Ridley[37], plays a significant role in shaping the dynamical response and energetic characteristics of the system near the EOC regime. Under appropriate circuit conditions, the system exhibits spontaneous, self-sustaining oscillatory dynamics at low DC currents on the order of 100 nanoamperes, more than three orders of magnitude lower than those in typical electrothermal implementations. To elucidate the underlying mechanisms, we developed a physics-based compact model incorporating filament growth and dissolution kinetics. SPICE simulations closely match experimental observations, supporting a consistent interpretation of EOC dynamics arising from coupled ionic transport and circuit capacitance. These findings establish diffusive memristors as an energy-efficient platform for neuromorphic and nonlinear dynamical computing, while providing physical insight into the emergence of locally active regimes in nanoionic systems.

Results and discussion

Edge of chaos dynamics in ion-driven diffusive memristors

In biological systems, neurons operate in a critical regime, where small changes in input stimuli can trigger action potentials. As illustrated in Fig. 1a, cortical neurons produce voltage spike trains that reflect the intrinsic excitability of the membrane. This behavior has been mathematically modeled by the Hodgkin-Huxley equations[3], in which coordinated sodium and potassium ion channel dynamics lead to regenerative depolarization. The FitzHugh-Nagumo model electronically simulated neural excitability through nonlinear dynamics introduced by small-signal voltage-controlled negative resistance using tunnel diodes[38,39]. More rigorous circuit-theoretic analyses have demonstrated that the ion channels in the Hodgkin-Huxley equations are better represented by memristors that are poised in the EOC[1,2].

Analogous spontaneous spiking with a constant current source is observed in ion-based diffusive memristors, as shown in the inset of Fig. 1c. The voltage-current *(V-I)* characteristics of the memristor exhibit NDR, which is significantly enhanced by a Ridley transition[37] to a state of lower power dissipation (and thus entropy production) as depicted in Fig. 1d, marking the system's transition to EOC dynamics.

To benchmark the energy efficiency of the diffusive memristor, we compare it with other reported EOC materials and devices, as summarized in Fig. 1e. The diffusive memristor presented in this work operates at significantly lower DC current and voltage levels than previously reported electrothermal systems such as NbO_2[19,40], VO_2[22], TiO_2[41], TaO_x[42], and $LaCoO_3$[43]. This low total (DC plus AC) power consumption (three orders of magnitude lower than electrothermal systems), together with its intrinsic fidelity to the stochastic characteristics of biological systems, highlights the potential of diffusive ionic dynamics for future neuromorphic computing architectures, where energy-efficient and adaptive signal generation is required.

Nonlinear device dynamics under current control

We characterized an ionically driven nanoscale solid-state device with dynamics analogous to those observed in biological systems. A symmetric metal–insulator–metal (MIM) architecture with a vertically stacked Pt/Ag/SiO_2/Ag/Pt structure was fabricated, as verified by depth profile analysis through the film (Supplementary Fig. 5) and secondary X-ray imaging (Supplementary Fig. 6). This spatial distribution of Ag enabled ion migration kinetics and facilitated the emergence of nonlinear dynamics. After fabrication, wire bonding was performed to connect the device terminals to the external measurement circuitry.

To rigorously characterize and capture the nonlinear dynamics of the device, which cannot be accurately measured by commonly used commercial instruments, we designed a customized measurement circuit (Supplementary Fig. 7). A source-measure unit (SMU) was used only as a quasi-DC input current source, and capacitors with varying capacitance values were connected in parallel with the memristor to modulate its nonlinear response, thereby enabling accurate measurement of spiking and oscillatory behavior. This configuration allows fine-tuning of the circuit's temporal integration properties. The output voltage signals were monitored in real time using a high-bandwidth oscilloscope, enabling direct observation of dynamical behavior under different circuit conditions.

To identify the input conditions required to access the NDR regime of the device, we performed voltage and current sweeps using the SMU under two different sweep modes (Fig. 1f). Specifically, current responses to voltage sweeps (*I-V* curve, red) and voltage responses to current sweeps (*V-I* curve, blue) were measured, corresponding to voltage-sourced and current-sourced conditions, respectively. Under voltage-sourced conditions (red curve), which have been the default for previous diffusive memristor studies[25], the device exhibited threshold switching behavior typically observed in diffusive memristors (Supplementary Fig. 8)[25,44]. At low voltages, the current increased gradually in proportion to the applied voltage. However, once the voltage exceeded a critical threshold, the current jumped rapidly until reaching the preset compliance, which limited the maximum current flowing through the device (Fig. 1f). In this case, no indication of NDR behavior was observed. In contrast, the current-sourced measurement (blue curve) exhibited a markedly different response. As the input current increased, the measured voltage reached a local maximum and then abruptly decreased, revealing a well-defined NDR regime. This sudden voltage collapse is a characteristic feature of the Ridley transition[37].

The distinct behaviors observed under the two biasing schemes arise from fundamental differences in system stability. In the voltage-sourced configuration, the current-voltage characteristic exhibits an

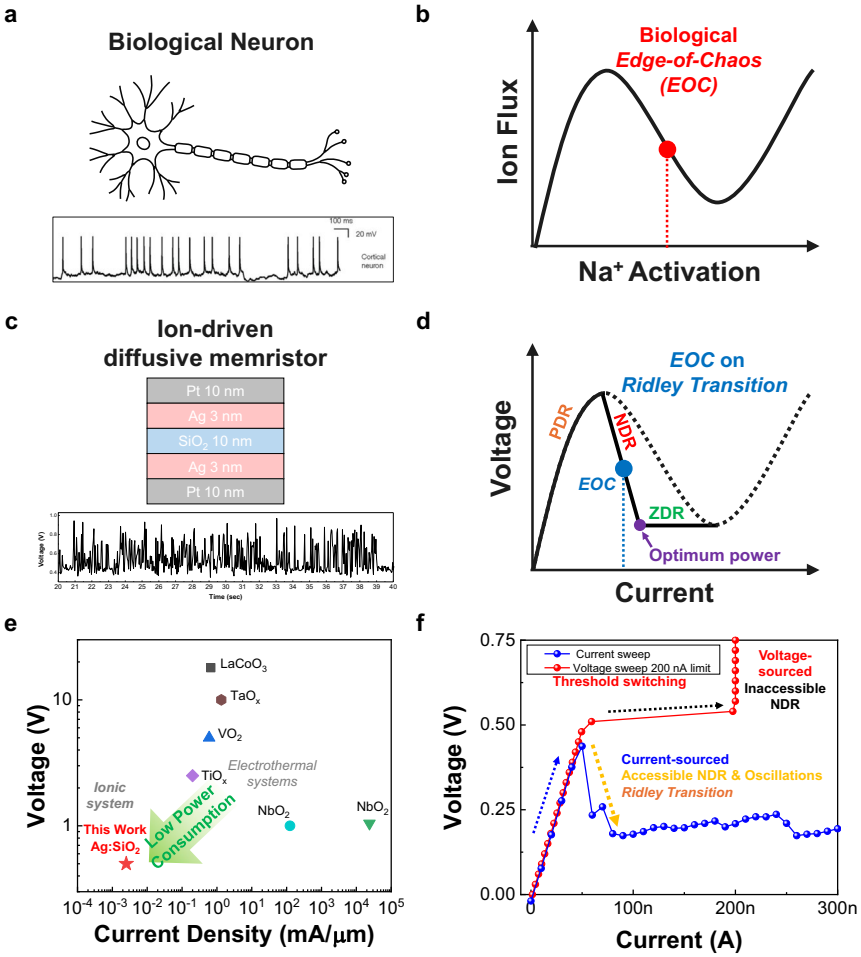


Fig. 1 | Edge of chaos dynamics in ion-driven diffusive memristors inspired by biological neurons. a Schematic of a biological neuron showing periodic spiking behavior. Spiking data reproduced from ref. 48 under a Creative Commons Attribution 3.0 license, https://creativecommons.org/licenses/by/3.0/. No changes were made. **b** Conceptual illustration of the quasi-static nonlinear ionic response in a biological neuron. The ordinate represents the Na^+ ionic flux (or equivalently, the Na^+-mediated ionic current) as a function of Na^+ channel activation. The EOC operating point corresponds to a locally active but stable regime, often associated with regions of negative differential resistance (NDR), where small perturbations can be strongly amplified. **c** Schematic of an Ag:SiO_2 film diffusive memristor illustrating ionic drift-diffusion through a conductive channel within a vertically stacked structure. Experimental voltage spikes induced by a 100-nanampere DC current input are shown below, demonstrating self-sustained dynamics. **d** Quasi-static nonlinear voltage-current response in the memristor, with the slope of the NDR enhanced by the Ridley transition determining the EOC regime. **e** Comparison of operating voltage and DC bias current density for various previously reported oscillatory materials and devices. The Ag:SiO_2 diffusive memristor presented in this work (marked by a star) operates at lower current density and voltage compared to previously reported systems, enabling low-power operation for neuromorphic applications. **f** Comparison of electrical characteristics under different sourcing conditions: the voltage-sourced *I-V* curve exhibits abrupt threshold switching, while the current-sourced *V-I* curve reveals an accessible and steep NDR regime.

'S-shaped' curve, where a single applied voltage may correspond to multiple possible current values (Supplementary Fig. 9a). This multi-valued regime is intrinsically unstable and cannot be sustained, causing the system to undergo abrupt threshold switching and rendering the NDR regime inaccessible in the presence of noise. In contrast, under current-sourced conditions, there exists a one-to-one correspondence between the input current and the measured voltage (Supplementary Fig. 9b), which ensures NDR accessibility.

A more in-depth study was conducted to examine the dynamic evolution of the system under current-source operation. The quasi-static DC *V–I* characteristics of the diffusive memristor were measured without an added external parallel capacitor; only the intrinsic and stray capacitances of approximately 10 pF were present (Fig. 2a). Initially, the device behaved as a passive high-resistance (~10 MΩ) ohmic conductor, equivalent to a constant positive differential resistance (PDR, yellow region). When the current reached 100 nA, the voltage peaked at 0.97 V and then decreased abruptly, exhibiting a NDR with an amplitude of approximately -20 MΩ (red region) to 0.36 V at a current of ~130 nA. Beyond this current, the voltage remained constant (zero differential resistance, ZDR) up to at least 500 nA (blue region). The NDR current region was also characterized by a sharp decrease in power dissipation, from ~100 nW to ~50 nW (Fig. 2b), and thus also entropy production. All of these behaviors (PDR, sharp NDR, and ZDR) were predicted by Ridley based on entropy production minimization[37]. By precisely controlling the DC source current at a constant value in the ~100 nanoampere range, the distinct conduction regimes of PDR, NDR and ZDR were selectively accessed in the memristor, revealing rich nonlinear dynamics in *V-t* curves.

To examine the reproducibility of this behavior, current sweeps were performed at different current sweep speeds, ranging from 200 nA s^{-1} to 2.5 nA s^{-1} (Supplementary Fig. 10). These measurements consistently revealed the Ridley transition and the associated NDR region within a narrow current window. At slower sweep speeds, the switching current was observed at slightly lower values, consistent with an increased probability of noise-assisted triggering of the instability due to the longer residence time at each current level.

https://doi.org/10.1038/s41467-026-74640-6

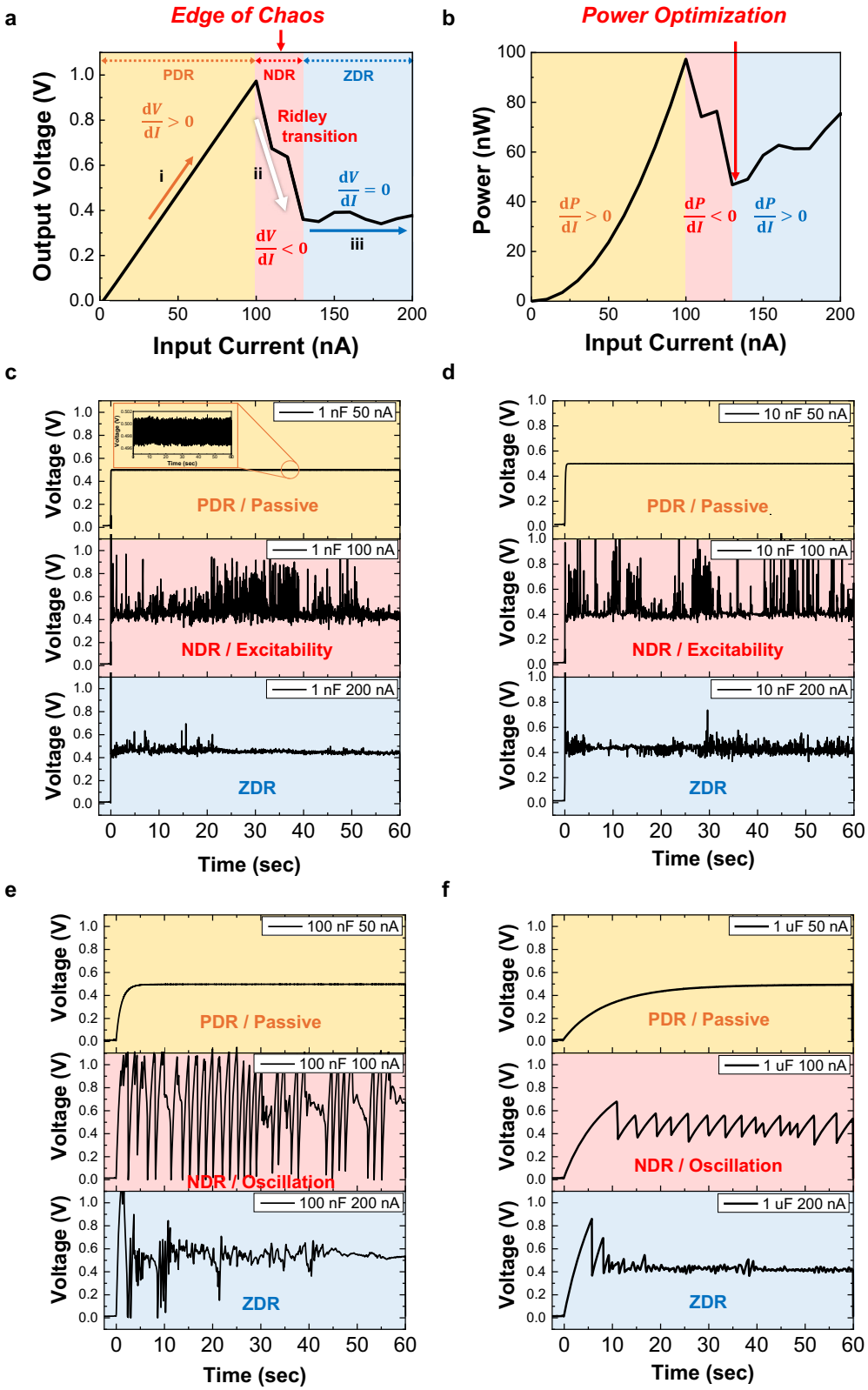


Fig. 2 | Electrical characterization of a diffusive memristor. a Quasi-static DC *V-I* characteristics of the diffusive memristor (current sweep rate 500 nA s^{-1}) without an intentionally added external parallel capacitor (i.e., only intrinsic and stray capacitances of ~10 pF are present), highlighting regimes of positive differential resistance (PDR), negative differential resistance (NDR), and zero differential resistance (ZDR), depending on the applied current. **b** Power vs. current corresponding to (**a**), showing that the Ridley transition significantly reduced the power dissipation and thus the entropy production in the device. **c, d** Time-dependent voltage (*V*–*t*) responses measured with parallel capacitances of (**c**) 1 nF and (**d**) 10 nF under different DC current biases. A 50 nA bias reveals low-noise PDR behavior, 100 nA results in excitable or noisy NDR, and 200 nA leads to the ZDR regime. **e, f** Time-dependent *V-t* responses measured with parallel capacitances of (**e**) 100 nF and (**f**) 1 μF under the different DC current biases. At 50 nA, the device is in the passive PDR regime; at 100 nA, it enters the NDR regime with spontaneous self-oscillations; and at 200 nA, it displays transient oscillations in ZDR.

Importantly, the overall form and abruptness of the transition remained unchanged, demonstrating that the observed features are intrinsic to the device physics rather than artifacts of sweep rate.

To confirm that the system also operates in the EOC, the key dynamic signatures of noise amplification (or excitability) and sustained oscillations were investigated[43]. Supplementary Video 1 shows oscilloscope traces of the voltage across the memristor as the current was scanned through the NDR region, revealing a large and abrupt increase in noise. Figure 2c–f show voltage vs. time (*V-t*) plots for fixed current biases and four different parallel capacitances.

When a small parallel capacitor (1 nF or 10 nF) was connected to the device (Fig. 2c and d), the voltage responded promptly to internal state transitions. In the PDR regime (50 nA current bias, top panel), the voltage rapidly saturated at ~0.5 V and remained passively stable over time after the current was applied, with a noise amplitude in the 4 mV range. For an applied input current in the NDR regime (100 nA, middle panel), the system exhibited high amplitude, irregular, high-frequency voltage spikes up to 0.4 V that persisted over time (Supplementary Video 2). These amplified fluctuations are a direct consequence of the excitability of the diffusive memristor, characterized by high sensitivity to various sources of noise in the system[43,45]. When the current was applied in the ZDR regime (200 nA, blue region), there was a single sharp voltage spike followed by a transient decay of the fluctuation amplitude.

In contrast, when a larger capacitor (100 nF or 1 μF) was used, the capacitance exceeded the critical threshold (see Supplementary Note 4) required for the onset of self-sustained oscillations[22] (Fig. 2e and f). In the PDR regime (50 nA current), the voltage gradually saturated at ~0.5 V due to the time constant from the large external capacitance and then remained passively stable over time. In the NDR regime (100 nA source current), the system exhibited pronounced self-sustained oscillations (Supplementary Video 3). These oscillations arose from the interplay between the internal state dynamics of the diffusive memristor and the charge-discharge behavior of the large external capacitor[22]. When the current was applied in the ZDR regime (200 nA), the system exited the EOC, and the voltage subsequently stabilized at a constant level after a few transient oscillations. These observations taken together demonstrate that the diffusive memristor operated in the EOC at room temperature and confirm the finite but relatively narrow region of the active EOC experimental parameter space, as noted by Chua[1]. This behavior contrasts with previously reported electrothermal EOC systems, such as $LaCoO_3$-based devices[43], where the amplified noise source is thermal excitations of electrons, leading to smaller amplitude and higher frequency signals. In the present Ag:SiO_2 diffusive memristor, the noise primarily comes from the effects of the drift and diffusion of ions, leading to large amplitudes and low frequencies. Nevertheless, the pronounced amplification of intrinsic noise in the NDR regime provides direct evidence of local activity consistent with the EOC state. Quantitative analyses of the transition from stochastic fluctuations to oscillatory dynamics based on power spectral density and autocorrelation of the $V(t)$ results for the diffusive memristor current biased in NDR are provided in Supplementary Note 2 and Supplementary Figs. 11 and 12.

To investigate the thermal impact on EOC dynamics, the device response was examined at elevated temperatures (Supplementary Fig. 13). The *V-I* characteristics measured without an added external capacitor at room temperature and 125 °C (Supplementary Fig. 13a) show that the NDR behavior was preserved at elevated temperature, while the onset of NDR shifted to lower current and lower voltage at 125 °C, consistent with thermally activated ionic transport. *V-t* curves measured in the NDR regime under a current bias of 100 nA with 1 μF capacitance (Supplementary Fig. 13b) revealed that the oscillations observed at room temperature disappeared completely at 125 °C. Although temperature is not an explicit state variable in this system (it is essentially a state parameter), it strongly affects ionic dynamics. At higher temperatures, the device continued to exhibit a steep NDR response but no longer operated in the EOC. This highlights that although NDR is a strong indicator of EOC, it is not a sufficient condition. This behavior parallels that of biological neurons, which can function only within a narrow temperature window.

Compact modeling of edge of chaos dynamics

To understand the EOC dynamics of a diffusive memristor at the atomic scale, a physics-based compact model was developed. Unlike computationally intensive full-physics methods such as density functional theory (DFT), molecular dynamics (MD), phase-field modeling, or kinetic Monte Carlo (kMC) simulations, this model provides a simplified yet effective framework for capturing the core physical processes governing device behavior[46]. Diffusive memristors are characterized by the coexistence of two key features: Ag nanoparticles embedded within the oxide dielectric that act as stable remnant structures, and transient conductive filaments that form and dissolve rapidly in response to external stimuli (Fig. 3a). These distinct elements play complementary roles in enabling rich dynamical behavior[25].

The model comprises two principal components that reflect the dual electronic transport mechanisms in the system. The first component is ohmic resistance, which accounts for transport through the metallic portion of the filament. This resistance is modeled as being proportional to the filament length, following Ohm's law. The second is tunneling resistance across nanoscale insulating gaps, which depends exponentially on the gap distance under low field tunneling conditions[47]. The total device resistance is expressed as the sum of these two components, consistent with the series configuration of a partially formed filament. To simulate time-dependent switching behavior, the model tracks the temporal evolution in the presence of noise in the internal state variables, specifically filament length and gap size, which are governed by ionic drift and diffusion. Further details of the compact model and its implementation are provided in Supplementary Note 3.

This dynamic framework captures the changes in voltage and resistance with increasing and decreasing current, allowing the compact model to accurately and efficiently reproduce key experimental signatures of the Ridley transition and EOC behavior in diffusive memristors, including excitability, self-sustained oscillations and nonlinear conduction regimes. In the *V-I* domain, it captures the sharp NDR associated with the Ridley transition and the ZDR regime, characterized by constant voltage despite increasing current (Fig. 3b). The simulated curves also show close agreement with experimental data under various parallel capacitance configurations (Supplementary Figs. 14–20 **and** Supplementary Table 2). In the *V-t* domain, the model captures the emergence of excitability and noise-amplification behavior under small parallel capacitance (Fig. 3c). In a visually striking representation, the channel length continually deviates from but always returns to its maximum stable length of ~95% of the SiO_2 film thickness (Fig. 3d **and** Supplementary Fig. 21), faithfully reproducing the hallmark feature of excitability as a transient departure from the steady state[48]. The simulations also reveal regime-specific dynamics in PDR and ZDR (Supplementary Figs. 22, 23 **and** Supplementary Table 3). The model further reproduces self-sustained voltage oscillations in the NDR regime (Fig. 3e, f**, and** Supplementary Fig. 24). The emergence of oscillations is governed by a critical capacitance, arising from a time-scale matching condition between the external RC time constant and the intrinsic ionic dynamics. This condition defines the transition from excitable fluctuations to sustained oscillations and is further analyzed using compact model simulations and bifurcation analysis (Supplementary Note 4 and Supplementary Fig. 25). The simulated evolution of the conductive channel during oscillation further illustrates how the filament length, remnant length, and total channel length dynamically vary over time. The model also reproduces distinct dynamic responses in the PDR and ZDR regimes depending on the source current

https://doi.org/10.1038/s41467-026-74640-6

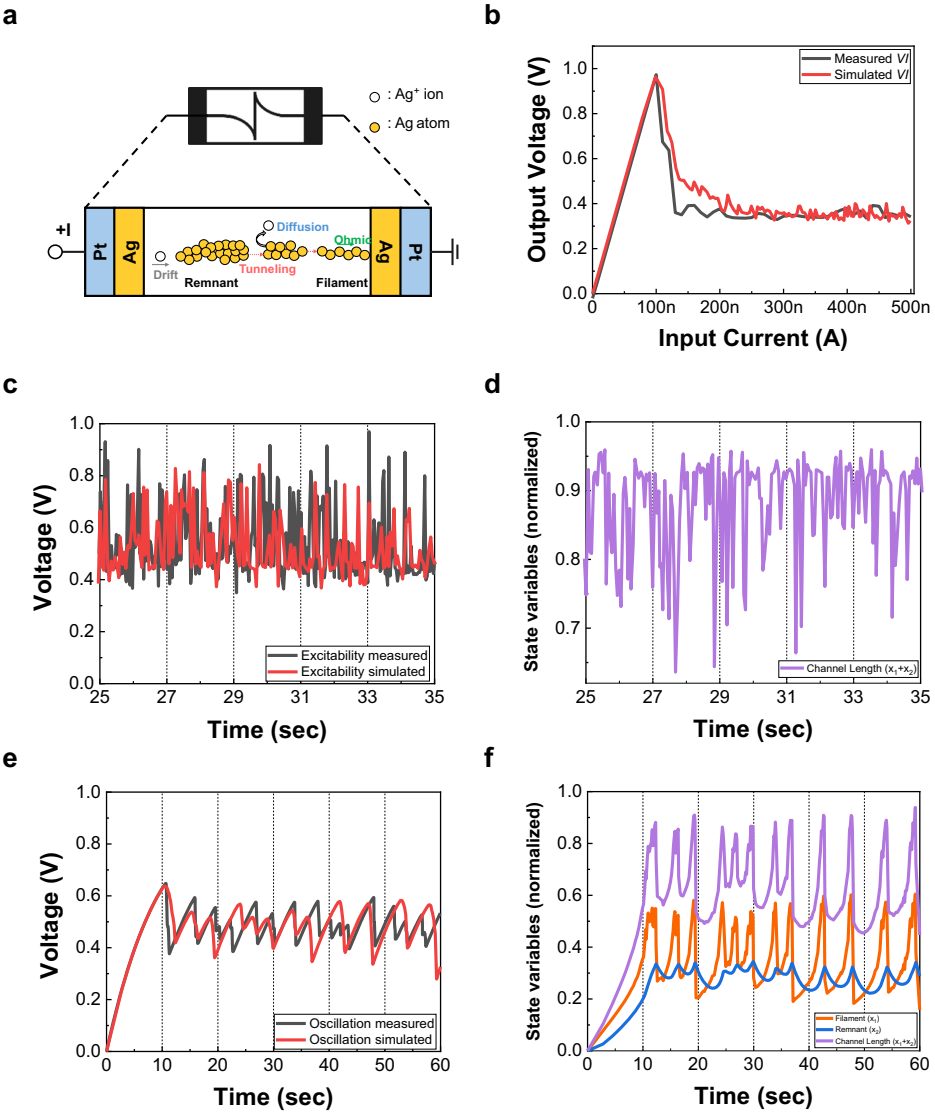


Fig. 3 | Compact model of edge of chaos dynamics in diffusive memristors revealing underlying dynamical mechanisms. a Schematic illustration of the compact model of a diffusive memristor operating in the EOC. **b** Comparison of measured and simulated *V-I* characteristics (current sweep rate 500 nA s^{-1}) showing the emergence of NDR in the forward scan and hysteresis on the reverse scan. **c** Comparison of measured and SPICE simulated time-domain voltage responses in the EOC regime showing excitability under a 1 nF capacitor and 100 nA current source, with noise introduced explicitly in the simulations. **d** Simulated evolution of the conductive channel length, defined as the sum of state variables, showing the excitability of the total channel length from the steady state. **e** Comparison of measured and SPICE simulated time-domain voltage responses in the EOC regime showing oscillations under a 1 μF capacitor and 100 nA current input. **f** Simulated evolution of the conductive channel during oscillation, showing filament, remnant, and total channel lengths.

magnitude (Supplementary Figs. 26 and 27), reliably simulates the temperature-dependent behavior (Supplementary Figs. 28 and 29) and the hysteresis on the reverse current scan (Fig. 3b).

Atomic-scale mechanisms of edge of chaos dynamics

Building on the insights provided by the compact model, an atomic-scale mechanism is proposed to explain the Ridley transition and EOC dynamics observed in diffusive memristors, (Fig. 4a). The device initially operates in the PDR regime, where the source current gradually increases the electric field across the dielectric. Once the field exceeds a critical threshold, Ag^+ ions drift toward the counter electrode and are reduced to metallic Ag, initiating the formation and extension of a conductive path. As this channel develops toward the opposing electrode, the device undergoes a Ridley transition into the NDR regime, in which the tunneling gap becomes sufficiently narrow to allow a sudden, sharp voltage and power drop with increasing current bias due to the rapid decrease in resistance. The resistance of the diffusive memristor was much higher than the quantum resistance (on the order of tens of kΩ) expected for a fully connected filament between the TE and BE, suggesting that a stable nanogap was formed to enable the establishment of a non-shorting conduction path[49]. In the subsequent ZDR regime, the conduction channel enters a quasi-steady state in which the tunneling gap continues to narrow, maintaining a nearly constant voltage even as the current increases. This results in minimal voltage variation despite increasing current, reflecting a dynamic balance between ionic drift and partial atomic Ag dissolution, and also confirming a prediction resulting from EPM by Ridley.

The self-sustained oscillations observed in the diffusive memristor in Fig. 2c and d arise from a closed-loop cycle of filament formation and dissolution, driven by atomic-scale ionic and electronic processes and reinforced at the circuit level by capacitor-mediated feedback (Fig. 4b). This oscillatory behavior progresses through four sequential stages, beginning with circuit-level dynamics and directly correlating them with the underlying atomic-scale mechanisms (Fig. 4c). (**i**) In the

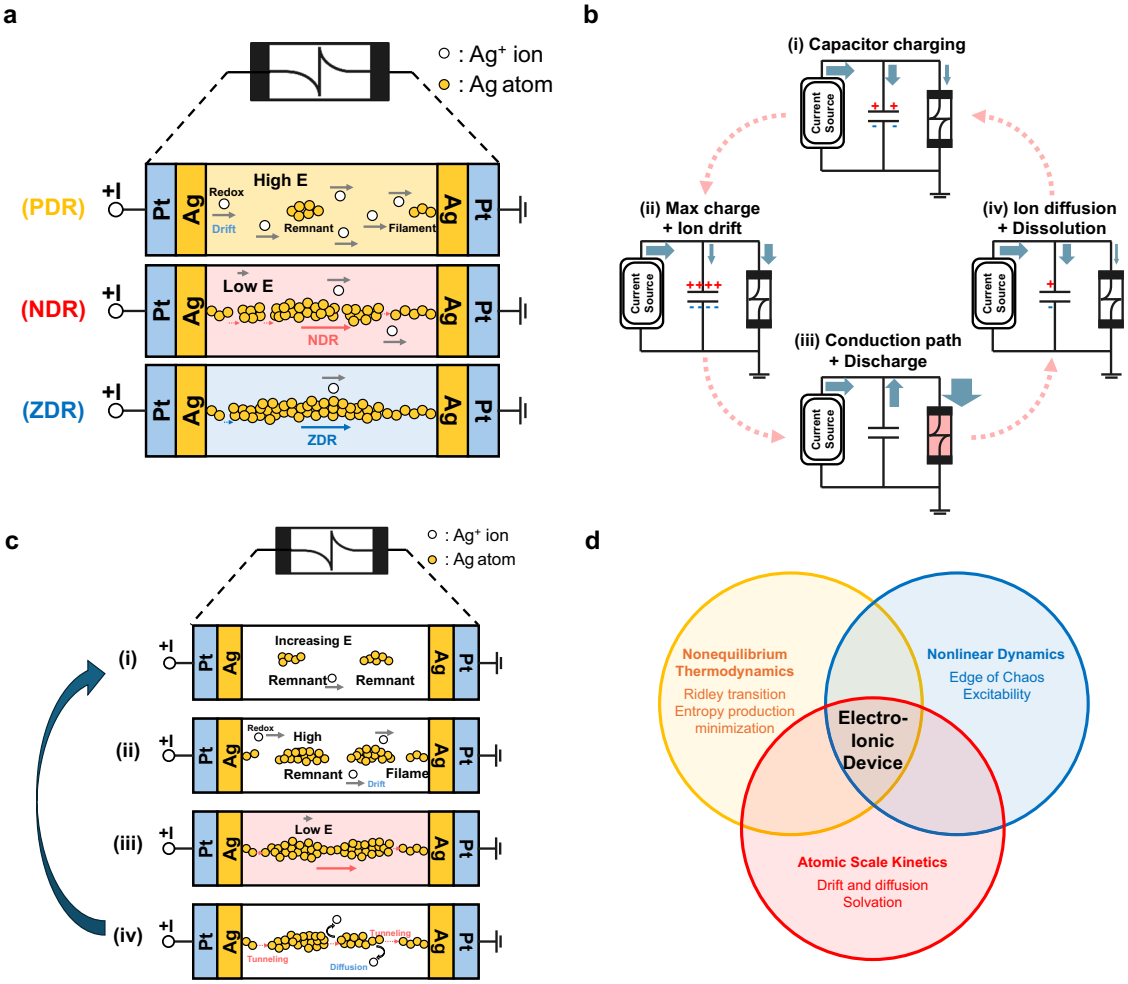


Fig. 4 | Atomic-scale mechanism of edge of chaos dynamics in diffusive memristors informed by compact model simulations. a Schematic illustration of atomic-scale steady-state PDR, NDR, and ZDR phenomena in a diffusive memristor. **b** Circuit-level depiction of the oscillatory mechanism under current-controlled operation with an external capacitor, illustrating the four key stages. **c** Schematic representation of atomic-scale oscillation dynamics in the diffusive memristor, showing the cyclic sequence. **d** Conceptual framework of electro-ionic devices, shown as a Venn diagram illustrating the intersection of nonequilibrium thermodynamics, nonlinear dynamics, and atomic-scale kinetics.

high-resistance state, the applied current bias causes the voltage across the device to rise as the circuit capacitor charges. At the atomic scale, this reflects the lack of a conduction channel, with the RC time constant controlling the slow development of an electric field across the SiO_2 layer. (**ii**) As the circuit capacitor approaches full charge, the electric field across the device intensifies, causing Ag^+ ions to drift toward the counter electrode, where they are reduced to metallic Ag. This leads to the growth of a conduction channel, either from pre-existing Ag nanoparticle remnants or newly nucleated sites near the electrode, initiating the transition into a more conductive state. (**iii**) As the conduction channel becomes sufficiently developed and the tunneling gap narrows to a critical width, the device exhibits an abrupt resistance drop, leading to a sharp voltage collapse and capacitor discharge. The formation of the conduction channel breaks the uniformity of ion distribution without the need for space charge confinement and its associated energy cost, as required for electrothermal memristors[37]. This behavior characterizes the NDR regime and corresponds to a transition from a weakly formed to a highly conductive state at the atomic scale. (**iv**) The voltage collapse weakens the electric field, and diffusion drives the dissolution of the filament. As the resistance recovers, the circuit capacitor begins to recharge, restoring the initial high-resistance state and initiating a new cycle. The dynamic interplay between ionic transport, electronic conduction, and capacitor feedback under constant-current bias gives rise to stable, self-sustaining oscillations without the need for an external periodic input or a physical inductor in the circuit. This atomic-scale kinetic mechanism is the physical route taken to minimize entropy production during the Ridley transition[37], leading to the emergence of a high-current-density conduction channel with high Ag concentration and sharp voltage and power decreases with increasing current. This also complements the nonequilibrium thermodynamic understanding of the Ridley transition[37], which includes the redistribution of current density through the Ag channel, a larger magnitude NDR, and thus significantly decreased power dissipation and Joule heating, which result from EPM. The larger magnitude NDR supports a robust EOC region, which in turn stabilizes the minimum entropy production state (Fig. 4d).

For five decades, the consensus has been that the minimum-entropy-production state in an electronic circuit is unstable, based on a DC resistance analysis by Landauer[50]. However, the experimental results of this paper and others[22,43] conclusively demonstrate that under current-source conditions for a current-controlled NDR, a Ridley transition is observed and is stable. The resolution to this contradiction is Chua's proof of the existence of globally stable EOC[23], which utilized a small-signal circuit theoretic analysis to identify limited regions of stability in the complex impedance of a dynamical system.

Thus, EPM and EOC are intimately linked, with a Ridley transition providing a steep enough NDR to support EOC[20], and EOC stabilizing the minimum entropy production state. While previous studies have demonstrated computational efficiency at the edge of chaos for non-trivial tasks[15,16,51], our results further suggest that operation near the EOC can also confer thermodynamic efficiency at the device level, as reflected by reduced entropy production associated with the observed dynamics.

The departure of the diffusive memristor from the EOC regime at higher temperatures is attributed to enhanced ionic mobility, which accelerates ion migration and overwhelms the temporal feedback required to sustain oscillations. At high temperatures, ions respond more rapidly to the applied field, eliminating the intrinsic delay that normally allows capacitive charge accumulation and release. Consequently, the feedback loop collapses, and the system converges to a passive conduction state rather than sustaining oscillatory dynamics. Consistent with this observation, *V-I* characteristics acquired at 25 °C and 125 °C (Supplementary Fig. 13b) show that the critical current required to enter the NDR regime decreases with elevated temperature, and after the sharp NDR transition, the device remains in the ZDR state at a lower voltage compared to room temperature, even as the current continues to rise.

These results experimentally verify EOC dynamics in an ionic-based diffusive memristor. The observation of a Ridley transition that decreases the power dissipation of the quasi-static DC *V-I* characteristic as a result of an increased amplitude NDR, followed by excitability, noise amplification, and self-sustained oscillations in the time domain, provides compelling evidence that a properly current-biased diffusive memristor operates within a regime of minimized entropy production that supports a Chua-defined EOC framework.

Despite millisecond spike durations arising from integrative ionic transport, the device operates at sub−1 V amplitudes and ~100nA DC current levels, maintaining nanowatt-scale baseline total power dissipation, approximately three orders of magnitude lower than that of electrothermal oscillatory devices. Integration of the measured *V-t* traces reveals spike energies in the few-nanojoule regime, demonstrating that complex nonlinear dynamics can be sustained at a low energetic cost.

When stabilized in the locally active regime associated with the EOC dynamics, the diffusive memristor exhibits intrinsically amplified stochastic fluctuations at low power. Such behavior is particularly attractive for noise-assisted optimization and probabilistic computing, where controlled fluctuations are constructively exploited rather than suppressed[19]. Unlike electro-thermal stochastic systems, the observed fluctuations emerge naturally from ionic diffusion and volatile filamentary dynamics, eliminating the need for large thermal activation or external noise sources. In probabilistic computing frameworks, including Hopfield and Ising networks, stochastic units with bias-tunable switching probabilities enable noise-assisted exploration of the energy landscape, facilitating escape from local minima and improving convergence toward low-energy states[19]. The intrinsic stochastic switching of the volatile ionic channel can therefore function as a compact on-chip stochastic element, analogous to probabilistic bits (p-bits)[52] used in stochastic optimization and sampling architectures, where each unit produces a binary output with a bias-dependent switching probability. In this context, the fluctuation-driven dynamics of the diffusive memristor provide a physical mechanism for generating the controlled stochasticity required for noise-assisted optimization and probabilistic inference, without reliance on electrothermal noise sources or externally injected randomness. These capabilities arise as a direct consequence of the locally active EOC regime enabled by the interplay of local activity, global stability, and ionic diffusion-driven volatility in the diffusive memristor[19].

To gain deeper insight into the underlying atomic-scale mechanisms, we significantly improved and extended a compact model that incorporates both metallic conduction through localized pathways and tunneling transport across nanoscale gaps. Implemented in SPICE, the model successfully reproduces key features of the experimental observations, notably the Ridley transition and excitability, effectively linking atomic-scale ionic dynamics with macroscopic nonlinear behavior. Such capabilities may provide a pathway to compact, energy-efficient neuromorphic hardware in which complex dynamics are accessed and modulated via nanoscale ionic transport rather than bulky or energy-intensive components.

Methods

Memristor fabrication

Diffusive memristors were fabricated on Si substrates with a 1.0 μm thermally grown oxide. The bottom electrodes were formed by e-beam evaporation through shadow masks, consisting of a 20 nm Pt layer capped with 3 nm of Ag. A 10 nm SiO_2 dielectric film was then deposited via RF sputtering under an Ar atmosphere. Subsequently, the top electrodes were deposited by e-beam evaporation through shadow masks, comprising a 3 nm Ag layer overlaid with 20 nm of Pt. The resulting devices exhibited a cross-point architecture with lateral dimensions of 10 μm × 10 μm.

Material characterization

XPS depth profiling was carried out on a PHI VersaProbe II instrument (Physical Electronics) using 2 kV Ar^+ ion sputtering, yielding a sputtering rate of approximately 0.5 nm/min. The depth-dependent elemental composition was analyzed by tracking the core-level signals of Pt 4 f, Ag 3 d, Si 2p, and O 1 s.

Electrical measurements

A customized measurement circuit was employed to rigorously characterize the EOC dynamics, which cannot be fully resolved using conventional commercial instruments. A high-resolution source/measurement unit (SMU) in Keysight B1500A served as a nanoampere-level current source, while external capacitors with varying capacitances were connected in parallel with the memristor to modulate the nonlinear response and suppress noise, enabling precise evaluation of oscillatory behavior. Circuit voltages and output signals were monitored in real time using a high-bandwidth Keysight MSOX3104T oscilloscope, allowing direct observation of voltage oscillations and dynamic transitions under different circuit conditions.

Compact model simulations

A compact model of the diffusive memristor was developed in LTspice, based on the atomic-scale dynamics of Ag conduction channels. The model includes the dynamics of active filaments, remnants, and stochastic shrinkage events. Simulations were carried out in a circuit consisting of a constant current source, intrinsic capacitance arising from the combined device and probe capacitances, an external capacitor, and a series resistor, reproducing the experimentally observed Ridley transition and oscillatory behavior. Further details are provided in Supplementary Note 3.

Data availability

The data and material resources supporting the findings of this study are available within the article and its Supplementary Information. The compact model used in this work is publicly available via Zenodo at https://zenodo.org/records/20150591. Source data are provided with this paper.

References

1. Chua, L., Sbitnev, V. & Kim, H. Neurons are poised near the edge of chaos. *Int. J. Bifurc. Chaos* **22**, 1250098 (2012).
2. Chua, L. O. Memristors on 'edge of chaos. *Nat. Rev. Electr. Eng.* **1**, 614–627 (2024).

3. Hodgkin, A. L. & Huxley, A. F. A quantitative description of membrane current and its application to conduction and excitation in nerve. *J. Physiol.* **117**, 500–544 (1952).
4. van Vreeswijk, C. & Sompolinsky, H. Chaos in Neuronal Networks with Balanced Excitatory and Inhibitory Activity. *Science (1979).* **274**, 1724–1726 (1996).
5. Miller, P. Dynamical systems, attractors, and neural circuits. *F1000Res* **5**, 992 (2016).
6. Legenstein, R. & Maass, W. Edge of chaos and prediction of computational performance for neural circuit models. *Neural Netw.* **20**, 323–334 (2007).
7. Beggs, J. M. The criticality hypothesis: how local cortical networks might optimize information processing. *Philos. Trans. R. Soc. A: Math., Phys. Eng. Sci.* **366**, 329–343 (2008).
8. O'Byrne, J. & Jerbi, K. How critical is brain criticality? *Trends Neurosci.* **45**, 820–837 (2022).
9. Strukov, D. B., Snider, G. S., Stewart, D. R. & Williams, R. S. The missing memristor found. *Nature* **453**, 80–83 (2008).
10. Chua, L. Memristor-The missing circuit element. *IEEE Trans. Circuit Theory* **18**, 507–519 (1971).
11. Chua, L., Sbitnev, V. & Kim, H. Hodgkin-Huxley axon is made of memristors. *Int. J. Bifurc. Chaos* **22**, 1230011 (2012).
12. Kim, S. J. et al. Linearly programmable two-dimensional halide perovskite memristor arrays for neuromorphic computing. *Nat. Nanotechnol.* **20**, 83–92 (2025).
13. Kim, S. J., Kim, S. B. & Jang, H. W. Competing memristors for brain-inspired computing. *iScience* **24**, 101889 (2021).
14. Im, I. H., Kim, S. J. & Jang, H. W. Memristive devices for new computing paradigms. *Adv. Intell. Syst.* **2**, 2000105 (2020).
15. Nishioka, D. et al. Edge-of-chaos learning achieved by ion-electron–coupled dynamics in an ion-gating reservoir. *Sci. Adv.* **8**, 10.1126/sciadv.ade1156 (2022).
16. Hochstetter, J. et al. Avalanches and edge-of-chaos learning in neuromorphic nanowire networks. *Nat. Commun.* **12**, 4008 (2021).
17. Gibson, G. A. et al. An accurate locally active memristor model for S-type negative differential resistance in NbOx. *Appl. Phys. Lett.* **108**, https://doi.org/10.1063/1.4939913 (2016).
18. Pickett, M. D., Medeiros-Ribeiro, G. & Williams, R. S. A scalable neuristor built with Mott memristors. *Nat. Mater.* **12**, 114–117 (2013).
19. Kumar, S., Strachan, J. P. & Williams, R. S. Chaotic dynamics in nanoscale NbO2 Mott memristors for analogue computing. *Nature* **548**, 318–321 (2017).
20. Brown, T. D., Kumar, S. & Williams, R. S. Physics-based compact modeling of electro-thermal memristors: Negative differential resistance, local activity, and non-local dynamical bifurcations. *Appl. Phys. Rev.* **9**, https://doi.org/10.1063/5.0070558 (2022).
21. Yi, W. Nonlinear dynamics and stability analysis of locally active Mott memristors using a physics-based compact model. *Front. Mater.* **12**, https://doi.org/10.3389/fmats.2025.1465852 (2025).
22. Brown, T. D. et al. Electro-thermal characterization of dynamical vo 2 memristors via local activity modeling. *Adv. Mater.* **35**, https://doi.org/10.1002/adma.202205451 (2023).
23. Chua, L. O. Local activity is the origin of complexity. *Int. J. Bifurc. Chaos* **15**, 3435–3456 (2005).
24. Yi, W. et al. Biological plausibility and stochasticity in scalable VO2 active memristor neurons. *Nat. Commun.* **9**, 4661 (2018).
25. Wang, Z. et al. Memristors with diffusive dynamics as synaptic emulators for neuromorphic computing. *Nat. Mater.* **16**, 101–108 (2017).
26. Zhao, R. et al. Memristive ion dynamics to enable biorealistic computing. *Chem. Rev.* **125**, 745–785 (2025).
27. Im, I. H. et al. Controlling threshold and resistive switch functionalities in ag-incorporated organometallic halide perovskites for memristive crossbar array. *Adv. Funct. Mater.* **33**, 2211358 (2023).
28. Valov, I. Redox-based resistive switching memories (rerams): electrochemical systems at the atomic scale. *ChemElectroChem* **1**, 26–36 (2014).
29. Valov, I., Waser, R., Jameson, J. R. & Kozicki, M. N. Electrochemical metallization memories—fundamentals. *Appl., prospects Nanotechnol.* **22**, 254003 (2011).
30. Midya, R. et al. Artificial Neural Network (ANN) to Spiking Neural Network (SNN) Converters Based on Diffusive Memristors. *Adv. Electron. Mater.* **5**, (2019).
31. Rao, M. et al. Timing Selector: Using Transient Switching Dynamics to Solve the Sneak Path Issue of Crossbar Arrays. *Small Science* **2**, https://doi.org/10.1002/aelm.201900060 (2022).
32. Yoon, J. H. et al. An artificial nociceptor based on a diffusive memristor. *Nat. Commun.* **9**, 417 (2018).
33. Im, I. H. et al. Halide Perovskites-Based Diffusive Memristors for Artificial Mechano-Nociceptive System. *Adv. Mater.* **36**, 10.1002/adma.202307334 (2024).
34. Wang, M. et al. S-Type Negative Differential Resistance in Semiconducting Transition-Metal Dichalcogenides. *Adv. Electron. Mater.* **5**, https://doi.org/10.1002/aelm.201800853 (2019).
35. Kim, S. J. & Yang, J. J. The critical role of thermodynamics in memristors. *Device* **2**, 100625 (2024).
36. Ascoli, A., Slesazeck, S., Mahne, H., Tetzlaff, R. & Mikolajick, T. Nonlinear dynamics of a locally-active memristor. *IEEE Trans. Circuits Syst. I: Regul. Pap.* **62**, 1165–1174 (2015).
37. Ridley, B. K. Specific negative resistance in solids. *Proc. Phys. Soc.* **82**, 954–966 (1963).
38. FitzHugh, R. Impulses and physiological states in theoretical models of nerve membrane. *Biophys. J.* **1**, 445–466 (1961).
39. Nagumo, J., Arimoto, S. & Yoshizawa, S. An Active Pulse Transmission Line Simulating Nerve Axon. *Proc. IRE* **50**, 2061–2070 (1962).
40. Ascoli, A. et al. On Local Activity and Edge of Chaos in a NaMLab Memristor. *Front. Neurosci.* **15**, 10.3389/fnins.2021.651452 (2021).
41. Alexandrov, A. S. et al. Current-controlled negative differential resistance due to Joule heating in TiO2. *Appl. Phys. Lett.* **99**, https://doi.org/10.1063/1.3660229 (2011).
42. Goodwill, J. M., Sharma, A. A., Li, D., Bain, J. A. & Skowronski, M. Electro-Thermal Model of Threshold Switching in TaO_x -Based Devices. *ACS Appl. Mater. Interfaces* **9**, 11704–11710 (2017).
43. Brown, T. D. et al. Axon-like active signal transmission. *Nature* **633**, 804–810 (2024).
44. Midya, R. et al. Anatomy of Ag/Hafnia-Based Selectors with 10^{10} Nonlinearity. *Adv. Mater.* **29**, 1604457 (2017).
45. Chua, L. Memristor, Hodgkin–Huxley, and Edge of Chaos. *Nanotechnology* **24**, 383001 (2013).
46. Wang, T. et al. A faithful and compact diffusive memristor model. *IEEE Trans. Circuits Syst. Artif. Intell.* **1**, 141–148 (2024).
47. Simmons, J. G. Generalized formula for the electric tunnel effect between similar electrodes separated by a thin insulating film. *J. Appl. Phys.* **34**, 1793–1803 (1963).
48. Rossant, C. et al. Fitting neuron models to spike trains. *Front. Neurosci.* **5**, 10.3389/fnins.2011.00009 (2011).
49. Yi, W. et al. Quantized conductance coincides with state instability and excess noise in tantalum oxide memristors. *Nat. Commun.* **7**, 11142 (2016).
50. Landauer, R. Stability and entropy production in electrical circuits. *J. Stat. Phys.* **13**, 1–16 (1975).
51. Tsunegi, S. et al. Information Processing Capacity of Spintronic Oscillator. *Adv. Intelligent Syst.* **5**, https://doi.org/10.1002/aisy.202300175 (2023).
52. Camsari, K. Y., Faria, R., Sutton, B. M. & Datta, S. Stochastic p-Bits for Invertible Logic. *Phys. Rev. X* **7**, 031014 (2017).

Author contributions

S.J.K., R.S.W., and J.J.Y. conceived the project. S.J.K. fabricated and characterized the devices, performed model simulations, and analyzed the overall results. T.W. and D.R. performed the compact model simulations and the Lyapunov analyses, which were guided by F.C. R.Z. assisted with device fabrication. Y.X. and J.Z. assisted in analyzing the experimental results. R.S.W. and J.J.Y. supervised the project. The manuscript was primarily written by S.J.K., R.S.W., and J.J.Y., with significant input from A.A. and F.C. All authors discussed the results and provided feedback on the manuscript throughout all stages.

Funding

The authors thank the following funding sources: U.S. Air Force Office of Scientific Research (grant no. FA9550-24–1-0322), Army Research Office (grant nos. W911NF2120128, W911NF1810268), and National Science Foundation (grants nos. 2240407, 2036359).

Competing interests

The authors declare no competing interests.

Additional information

Supplementary information The online version contains supplementary material available at https://doi.org/10.1038/s41467-026-74640-6.

Correspondence and requests for materials should be addressed to R. Stanley Williams or J. Joshua Yang.

Peer review information *Nature Communications* thanks Leon Chua, Cheol Seong Hwang, Zdenka Kuncic and the other anonymous reviewer(s) for their contribution to the peer review of this work. A peer review file is available.

Reprints and permissions information is available at http://www.nature.com/reprints

Publisher's note Springer Nature remains neutral with regard to jurisdictional claims in published maps and institutional affiliations.

Open Access This article is licensed under a Creative Commons Attribution-NonCommercial-NoDerivatives 4.0 International License, which permits any non-commercial use, sharing, distribution and reproduction in any medium or format, as long as you give appropriate credit to the original author(s) and the source, provide a link to the Creative Commons licence, and indicate if you modified the licensed material. You do not have permission under this licence to share adapted material derived from this article or parts of it. The images or other third party material in this article are included in the article's Creative Commons licence, unless indicated otherwise in a credit line to the material. If material is not included in the article's Creative Commons licence and your intended use is not permitted by statutory regulation or exceeds the permitted use, you will need to obtain permission directly from the copyright holder. To view a copy of this licence, visit http://creativecommons.org/licenses/by-nc-nd/4.0/.

© The Author(s) 2026